

Effect of the hatch spacing in laser powder bed fusion on the AlSi₇Mg aluminum alloy cutting forces and surface finish after turning

GHINATTI Edoardo^{1,a*}, BERTOLINI Rachele^{1,b}, GHIOTTI Andrea^{1,c},
BRUSCHI Stefania^{1,d*}

¹Via Venezia 1, 35151, Padova, Italy

^aedoardo.ghinatti@phd.unipd.it, ^brachele.bertolini@unipd.it, ^candrea.ghiotti@unipd.it,
^dstefania.bruschi@unipd.it

Keywords: Aluminum Alloy, Laser Powder Bed Fusion, Machining

Abstract. Applying additive manufacturing (AM) technologies in fabricating aluminum alloy automotive components can significantly enhance vehicle light-weighting through optimized design. By varying the AM process parameters, the resultant microstructure can be substantially altered, even post-heat treatment. Given that machining operations remain essential in many applications, understanding the impact of the AM parameters on the machining performances is vital. This paper explores how hatch spacing in laser powder bed fusion (LPBF) process affects the machinability of the AlSi₇Mg aluminum alloy, in terms of cutting forces and machined surface roughness, providing a correlation with the microstructure induced by both the AM and heat treatment steps. In particular, the research reveals that the larger the hatch spacing the smoother the machined surface, underlining the critical role of this LPBF parameter in determining the final surface quality.

Introduction

Laser powder bed fusion (LPBF) is a widely utilized additive manufacturing (AM) technology used to 3D print complex-geometry shapes that are unachievable through conventional manufacturing methods [1]. This technique is particularly employed for printing aluminum alloys, especially AlSiMg alloys, which present an optimal blend of strength, corrosion resistance, and affordability [2].

The properties of components fabricated through LPBF are determined by the complex melting and solidification stages they undergo, which, in turn, are significantly affected by the chosen process parameters. To achieve a better quality in these components, it is crucial to understand how the various AM parameters, such as the hatch spacing, influence the melting and solidification patterns, which, finally, determine the part microstructural features.

In [3], the Authors developed an improved three-dimensional transient heat transfer model to study the effects of both the hatch spacing and laser spot overlapping on the temperature distribution and molten pool behavior when printing AlSi₁₀Mg. It was observed that an increase in the hatch spacing leads to a decrease of the temperature on the powder bed. Notably, the hatch spacing influences not only the temperature of the melting pool, but also its distribution, as well as the molten pool's measured length, width, and depth. Finite element simulations showed that increasing the hatch spacing from 0.4 to 0.6 mm reduces the melt pool's width from 0.409 mm to 0.356 mm as well as its depth from 0.273 mm to 0.240 mm. In [4], the outcomes of the LPBF process carried out on the AlMgScZr alloy using different hatch distances were extensively studied, focusing on various aspects such as densification behavior, melting mode, crystallographic orientation, evolution of the grain boundary angle misorientation, and part tensile properties. The findings indicate that the densification improved at decreasing hatch distance, while the grain size increased due to the elevated cooling rate.

Since first introduction of the LPFB technology, its process parameters have been extensively varied to optimize the printed part properties and thus increase the feasibility of its employment in different sectors. However, there remains a limited number of studies on how the AM-induced microstructure can affect the AM part machinability.

In a previous work by the Authors [5], the effect of the microstructural anisotropy induced by LPBF carried out using various scanning strategies was evaluated when turning Ti6Al4V LPBF parts. Specifically, under constant laser power and bed fusion process parameters, different scanning strategies, namely stripes and chessboard patterns, were employed. The results indicated that altering the scanning strategy significantly affects the part mean grain size. For instance, the chessboard strategy resulted in a 32% reduction in grain size compared to the stripes one. Consequently, the micro-hardness of parts produced with the chessboard strategy was 17% higher than those produced with the stripes one. These variations in scanning strategy also influenced the surface finish of the machined samples: the stripes scanning strategy led to rougher and more uneven surfaces compared to the chessboard one.

The influence on tool wear and surface topography during milling LPBF Ti6Al4V parts at various growth inclination angles was examined in [6]. Tool wear and surface roughness were observed to decrease with a reduction in the inclination angle. This decrease was attributed to the influence of weak discontinuity zones along the build direction (BD), which facilitate the material removal when favorably oriented relative to the cutting tool's edge.

In [7], the BD significant impact on the machinability of AM stainless steels was demonstrated. AISI 316L stainless steel was fabricated using a high-power laser with a large spot size along various build directions. The machinability during milling was evaluated based on the cutting forces, surface finish, and tool wear at different cutting speeds. Post-additive manufacturing characterization revealed that the cross-section at 0° with respect to the BD had higher hardness than the vertical section at 90°. This resulted in higher cutting forces of the samples at 0° with respect to the BD compared to those at 90°, highlighting the anisotropy in machinability due to the high-power direct laser deposition process. This anisotropy also affected the machined surface finish, being the samples fabricated at 0° with respect to the BD rougher than those at 90°.

As demonstrated in the previously mentioned publications, while some researchers have explored the machinability of AM parts, none have specifically addressed the impact that AM parameters, which can induce microstructural anisotropy, can have on turning outcomes. To this aim, the present paper evaluates the impact of hatch spacing in LPBF on the machinability of the AlSi₇Mg aluminum alloy. For this purpose, a series of samples were fabricated at varying hatch spacing using LPBF and then subjected to heat treatment. Subsequent machining tests were conducted using fixed cutting parameters. The forces exerted during these tests were recorded, and the surface finish was evaluated. The results revealed a correlation between the alloy machinability and hatch spacing, indicating that smoother surfaces are achievable when using larger hatch spacings.

Materials and methods

LPBF of AlSi₇Mg Aluminum Alloy. In this study, AlSi₇Mg is the addressed aluminum alloy, in form of powders produced by gas atomization and subsequently printed using the LPBF process. The spherical powders, ranging in size from 20-63 μm, were supplied by Eckart™, Altana. The nominal chemical composition of the AlSi₇Mg powders is detailed in Table 1.

Table 1: AlSi₇Mg powder chemical composition.

Element	Si	Mg	Fe	Cu	Zn	Ti	Mn	Al
Value [%]	6.86	0.58	0.14	0.01	0.003	0.14	0.0004	Bal.

The AlSi₇Mg samples were printed using a Sisma™ MYSINT100 LPBF machine, equipped with a 200 W Yb fiber laser and a 55 μm spot diameter. The LPBF process was conducted in an inert atmosphere, specifically by insufflating argon, ensuring an oxygen level below 100 ppm in the working chamber. A preliminary experimental campaign was carried out to optimize the LPBF process parameters. For doing that, cubic samples of 10 mm side were printed at varying laser power, scanning speed, and hatch spacing, while energy density and layer thickness were set constant. The employed scanning strategy was a 3 mm x 3 mm chessboard pattern with layers inclined at 67° to each other, as per [8]. For each parameter combination, the samples density and porosities were measured. The density was assessed using the Archimedes' principle with a high-precision KERN™ ABT 120-5DM balance, while the porosities were evaluated through optical microscopy. The samples were cold-mounted, ground with up to 4000 grit-size abrasive papers, and polished using a synthetic cloth with 6, 3, and 1 μm diamond suspensions. After being cleaned with ethanol and dried, the polished surfaces were examined using a Keyence™ VHX-7000 optical microscope at high magnification. The porosity analysis was performed using a dedicated MATLAB™ script. The primary defects that were identified were lacks of fusion and gas entrapment porosities. The former are due to inadequate energy inputs, while the latter result from excessive energy leading to moisture and gas evaporation.

The optimized process parameters that lead to maximum densification and induce the minimum percentage of porosities were established as power (P) = 170 W, scanning speed (V) = 1056 mm/s, hatch spacing (h) = 150 μm, and layer thickness (Lt) = 30 μm. By using these parameters, three cylindrical samples (20 mm diameter and 70 mm height) were printed with varying hatch spacings, namely h = 125 μm, h = 150 μm, h = 175 μm. Afterwards, these cylinders underwent a T6 heat treatment, which includes solubilization at 535°C for 3 hours and artificial aging at 150°C for 6 hours, in order to relieve the LPBF-induced residual stresses and promote material strengthening through precipitate formation. The microstructure of the LPBF samples, both pre- and post-heat treatment, was analyzed using the aforementioned preparation method and Keller's etching solution. Differential scanning calorimetry (DSC) analyses with a DSC Q200™ calorimeter were conducted to assess differences among the samples, heating them from room temperature to 400°C at 10°C/min.

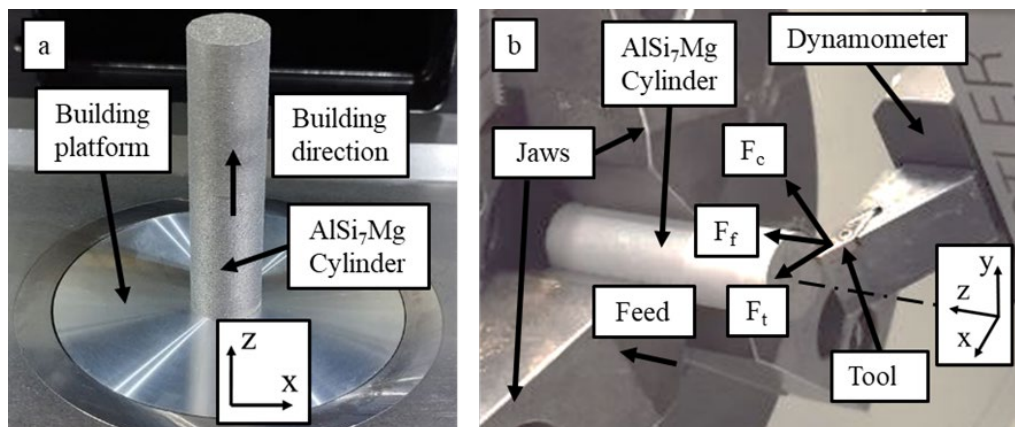


Fig. 1: a) As-built LPBF AlSi₇Mg cylinder and b) machining setup with the AlSi₇Mg cylinder mounted.

Machining of LPBF AlSi₇Mg Samples. The LPBF cylinders were utilized as workpieces in the turning trials, conducted on a Mori Seiki™ NL1500TM CNC lathe using conventional flooding lubrication. The employed cutting tool was the VCEX 11 03 01L-F 1125 turning inserts, procured from Sandvik Coromant™, whose main characteristics are detailed in Table 2.

Table 2. Turning tool specifications.

Parameter	Value
Substrate	Tungsten carbide
Coating	PVD TiAlN+TiAlN
Nose radius [mm]	0.1
Rake angle [°]	5°30′
Clearance angle [°]	7°
Cutting edge radius [mm]	0.01

The insert was attached to a SVJBL 2020 K11 - B1 tool holder, which was then secured to a 9129AA Kistler™ three-component piezoelectric dynamometer. As shown in Fig. 1, the cutting force (F_c), thrust force (F_t), and feed force (F_f) were measured during the tests. The force signals were captured at a sampling rate of 2500 Hz and processed using a 2nd-order low-pass filter with a 25 Hz cutoff frequency. The turning test parameters were consistent with the tool manufacturer's guidelines for finishing aluminum alloys, namely depth of cut (d) = 0.25 mm, cutting speed (V_c) = 200 m/min, and feed (f) = 0.03 mm/rev. Each experiment was conducted three times over a cutting length of 5 mm to ensure the reproducibility of the results.

Surface Finish Of The Machined LPBF AlSi₇Mg Samples. The topographies of the machined surfaces were acquired by using the Sensofar Plu Neox™ 3D optical profiler with a 20x Nikon™ confocal objective. The roughness parameters were computed by using the SensoVIEW™ software using the filtering procedure indicated in [9], namely a form removal process to remove the cylindrical form after turning, followed by a λ_s filter equal to 2.5 μ m, cut-off length λ_c equal to 0.8 mm, and sampling length of 4 mm. The arithmetic mean height (S_a), root mean square height (S_q), and total height (S_z) were the surface roughness parameters considered in the present study. While S_a is the conventional surface roughness parameter, S_q offers additional insight by quantifying the variance in surface height deviations, thereby providing a more comprehensive understanding of the surface texture and quality. S_z , on the other hand, measures the total extent of surface irregularities or deviations from a reference plane over a specific length.

Results and discussion

Microstructure of The LPBF AlSi₇Mg Samples. Fig. 2 displays the microstructure of the samples along the build direction and the scanning direction, also referred to as the x-z plane in Fig. 1, in their as-built state. After LPBF, macroscopic melting pools are clearly discernible in the low-magnification images. Each pool exhibits a fine microstructure in its central part and a coarser one at its boundaries. Notably, columnar grains along the build direction arise from localized heat dissipation by the laser. A notable variation in the melting pool size, related to hatch spacing, is evident. Reduced hatch spacing results in denser melting pools along the x direction, but fewer vertically, namely along the build direction, while the inverse is true for larger hatch spacings. This variation induces a microstructural anisotropy in the material, with the pool depths decreasing and widths increasing at increasing hatch spacings. Fig. 2 uses black and white arrows to distinguish between the pool depths and widths, respectively. This microstructural distribution is consistent with that found in [10], and is attributed to the varying energy distribution of the laser at different hatch spacings.

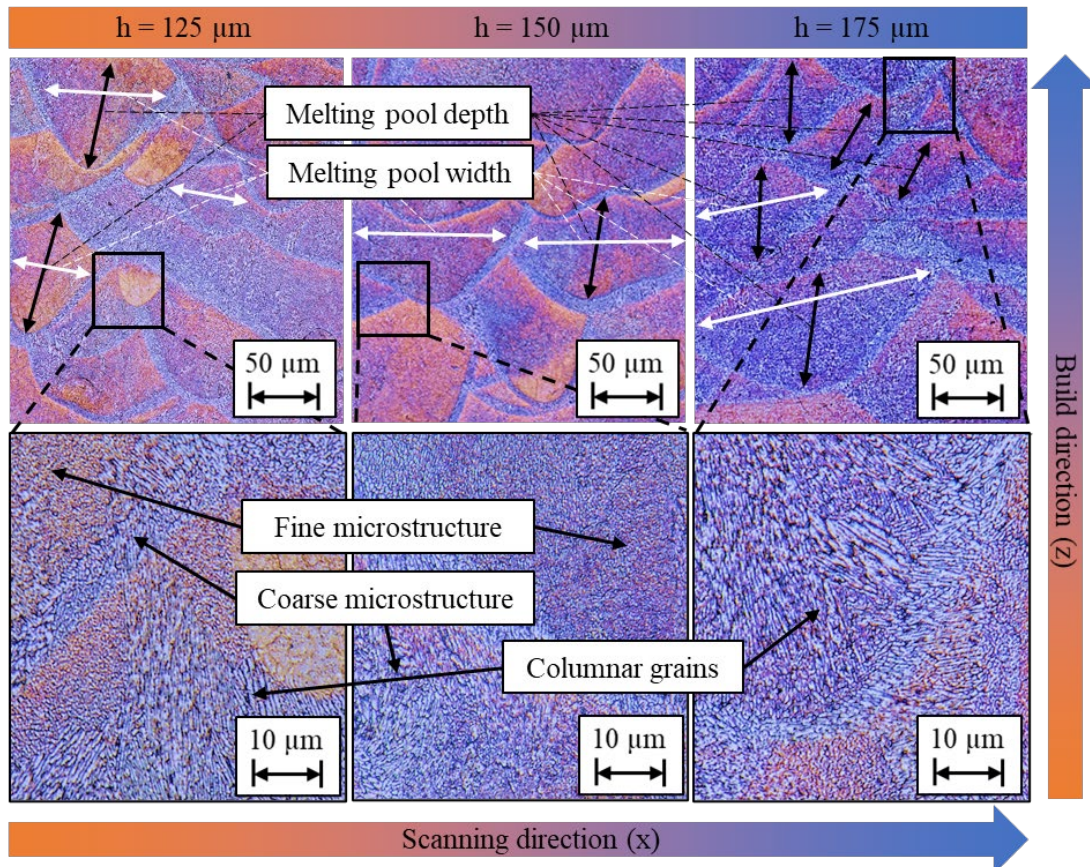


Fig. 2: Microstructure of the AlSi₇Mg LPBF samples along the building direction before heat treatment at varying hatch spacing.

As anticipated, along the x direction, a lower hatch spacing results in narrower melting pools due to increased overlap between adjacent scan lines. In the build direction, a lower hatch spacing delivers more energy to the material, raising the local temperature and reducing viscosity. This allows the material to spread more evenly downwards before solidifying. Conversely, at higher hatch spacings, as noted in [11], the opposite effect is observed.

The heat distribution variations caused by different hatch spacings also impact the cooling rates and solidification patterns, subsequently influencing the microstructure of the AlSi₇Mg LPBF samples. Observing a single melting pool in the magnified image of Fig. 2, it is evident that samples printed with the widest hatch spacing exhibit the coarsest grains. This is likely due to the slowest cooling rate at the highest hatch spacing, which facilitates grain growth.

After heat treatment, the microstructure becomes more homogeneous and less anisotropic, regardless of the hatch spacing, as shown in Fig. 3. The solubilization step enhances silicon precipitate formation, while aging promotes the development of nanometric-sized silicon particles [12], making the melting pools less distinguishable.

DSC analyses were conducted on the LPBF AlSi₇Mg samples at $h = 150 \mu\text{m}$ in the as-built condition, and after heat treatment for every value of hatch spacing to assess microstructural differences related to the precipitates, with results displayed in Fig. 4. All the DSC curves show an exothermic peak around 200°C-240°C, more pronounced for the sample in the as-built condition. The high enthalpy of this peak in the as-built alloy, attributed to Si precipitation, is due to the supersaturated state from the LPBF process and is drastically reduced after heat treatment [12].

This study notes a lower specific peak temperature compared to previous reports [12], possibly due to AM factors like residual stresses, porosity, and microstructural anisotropy, influencing the

DSC response and causing a peak shift after the heat treatment. Both the peak position and area vary depending on the hatch spacing used in LPBF, as indicated in Table 3. The peak temperature represents one of the maximum rates of formation or dissolution reactions, while the area under the peak correlates with the reaction heat and the phase volume fraction formed or dissolved, determined qualitatively by its enthalpy value [13]. Furthermore, the precipitate formation is closely linked to grain boundary density, as boundaries are nucleation sites due to their higher energy state. Thus, more intense precipitation occurs in samples with lower hatch spacing, evident in their finer microstructure and larger peak areas compared to those with $h = 175 \mu\text{m}$, indicating more material transforming.

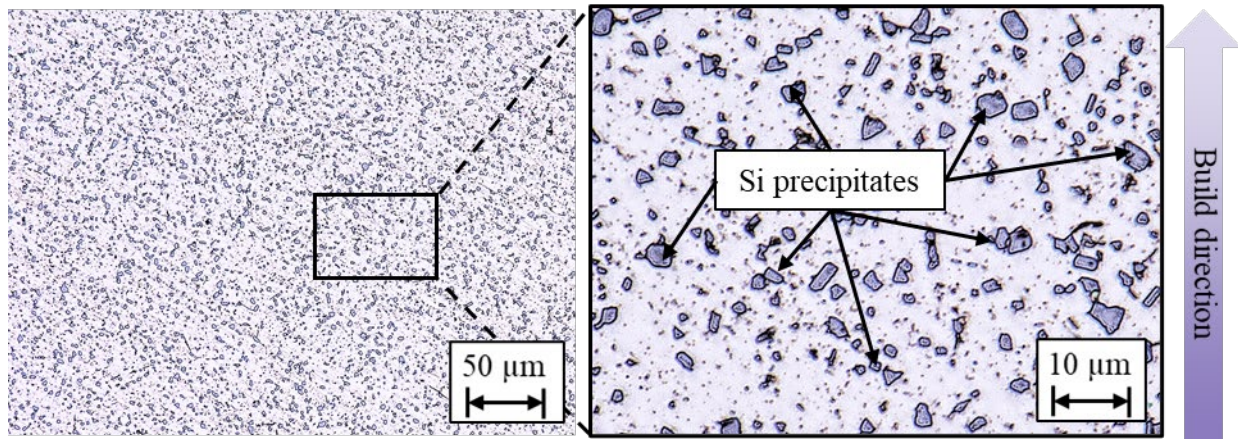


Fig. 3: Microstructure of the LPBF AlSi₇Mg samples fabricated with $h = 150 \mu\text{m}$ along the building direction after heat treatment.

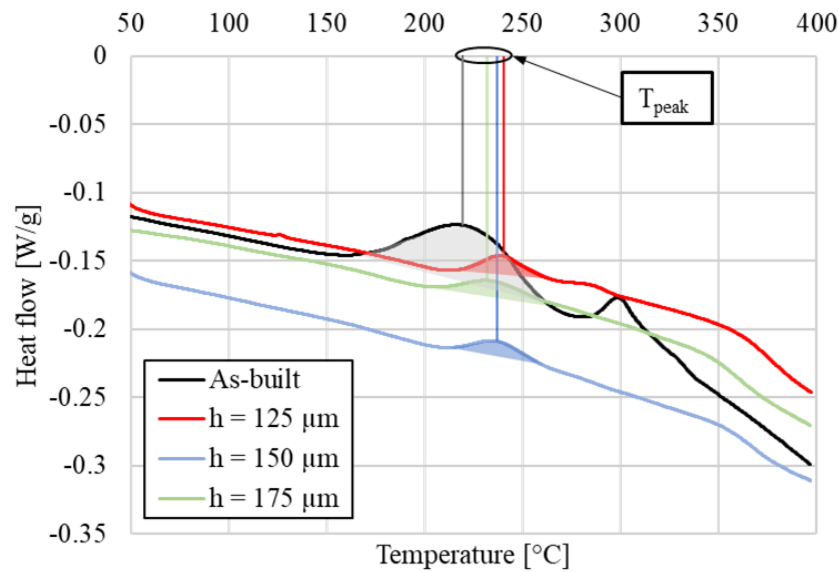


Fig. 4: DSC curves of the LPBF AlSi₇Mg samples before and after heat treatment at varying hatch spacing.

Table 3: Peak temperature and phase transformation enthalpy derived from Fig. 4.

Condition	As-built	Heat treated		
Hatch spacing [μm]	150	125	150	175
T_{peak} [$^{\circ}\text{C}$]	216	238	234	230
Phase transformation enthalpy [J/g]	15.23	2.22	2.19	2.14

Turning Forces. Fig. 5a displays an example of forces acquired when turning the LPBF AlSi7Mg samples manufactured with $h = 125 \mu\text{m}$, while Fig. 5b shows the mean values derived from Fig. 5a at varying hatch spacing. Considering the standard deviation, hatch spacing does not significantly impact the average force values. However, a higher variability in the cutting force values can be noted at decreasing hatch spacing. Given that the turning process is carried out at fixed parameters, this can be ascribed to the more heterogeneous microstructure obtained when using a lower hatch spacing. Large precipitates create indeed discontinuities for the cutting tool, resulting in increased force variability. In addition, higher precipitate density at lower hatch spacings contributes to increased variability in forces during cutting.

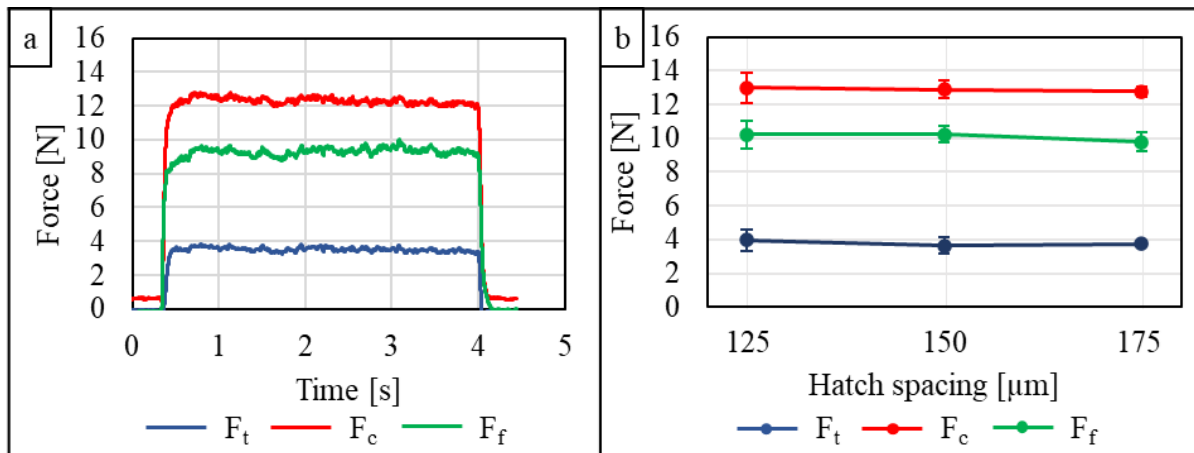


Fig. 5: (a) Forces recorded during turning of the LPBF AlSi7Mg samples fabricated with $h = 125 \mu\text{m}$, and b) mean values computed from a).

Surface Finish of The Machined LPBF AlSi7Mg Samples. Fig. 6a presents a comparison of the machined surface topography of the heat-treated LPBF AlSi7Mg samples before and after filtering fabricated using the intermediate hatch spacing. Fig. 6b shows the dependence of the surface roughness parameters on the hatch spacing. Generally, the larger the hatch spacing the better the surface quality. Specifically, the S_a , S_q , and S_z roughness values decrease by 32%, 34%, and 63% from the smallest to the largest hatch spacings, respectively. Consistent with the force results of Fig. 5, the samples fabricated with the smallest hatch spacing exhibit the greatest variability. A correlation with the microstructure is again evident: microstructures characterized by coarser grains and fewer precipitates are more easily machined, facilitating the attainment of smoother surfaces.

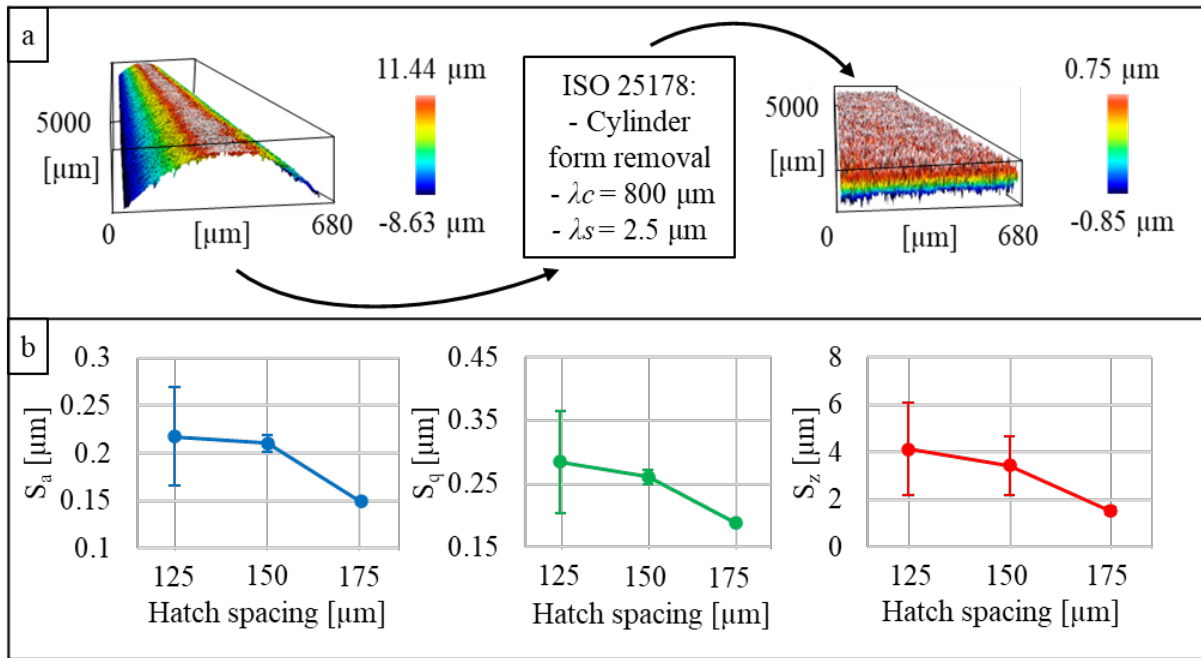


Fig. 6: (a) Surface topography of the LPBF AlSi₇Mg samples fabricated with $h = 150 \mu\text{m}$ before and after application of the filtering procedure, and b) surface roughness parameters at varying hatch spacing.

Conclusions

The present work focuses on the influence of hatch spacing varied during the LPBF process on the machinability of the AlSi₇Mg alloy, analyzing its effects on the cutting forces and machined surface roughness. The main results can be summarized as follows:

- A reduced hatch spacing results in denser melting pools along the x-direction, but fewer along the build direction; the opposite occurs with the largest hatch spacing.
- Larger hatch spacings result in samples with a coarser microstructure.
- Heat treatment significantly reduces anisotropy in the microstructure induced by the LPBF process.
- The density of the silicon precipitate density after heat treatment varies with the hatch spacing.
- Hatch spacing does not affect the average cutting force values, but influences their variability.
- Larger hatch spacings lead to smoother and more consistent surfaces, which is due to the different microstructure of the alloy, having a direct effect on the machining performances.

Future research endeavors will focus on assessing how the thickness of layers affects the machinability of AlSi₇Mg fabricated through LPBF. A thorough examination of the microstructure and distribution of precipitates will be conducted and correlated with the material's characteristics during cutting. It is anticipated that this will yield an optimal window of additive manufacturing process parameters, facilitating the production of dependable components that are easily machinable.

Acknowledgments

This work was supported by the European Union - NextGenerationEU (National Sustainable Mobility Center CN00000023, Italian Ministry of University and Research Decree n. 1033 - 17/06/2022, Spoke 11 - Innovative Materials & Lightweighting).

References

- [1] Wa. Abd-Elaziem, S. Elkatatny, A.E. Abd-Elaziem, M. Khedr, M. A. A. El-baky, M. A. Hassan, M. Abu-Okail, M. Mohammed, A. Järvenpää, T. Allam, A. Hamada, On the current research progress of metallic materials fabricated by laser powder bed fusion process: a review, *Journal of Material Research and Technology* 20 (2022) 681–707. <https://doi.org/10.1016/j.jmrt.2022.07.085>
- [2] H. Hyer et al., H. Hyer, L. Zhou, S. Park, G. Gottsfritz, G. Benson, B. Tolentino, B. McWilliams, K. Cho, Y. Sohn, Understanding the Laser Powder Bed Fusion of AlSi10Mg Alloy, *Metallography, Microstructure, and Analysis* 9 (2020) 484–502. <https://doi.org/10.1007/s13632-020-00659-w>
- [3] G. Nazami, S. Sahoo, Influence of hatch spacing and laser spot overlapping on heat transfer during laser powder bed fusion of aluminum alloy, *Journal of Laser Applications* 32 (2020) 042007. <https://doi.org/04200710.2351/7.0000157>
- [4] X. Li, Y. Liu, Z. Zhou, Influence of hatch distance on processing, microstructure and mechanical properties of AlMgScZr alloy fabricated by laser powder bed fusion, *Journal of Manufacturing Processes* 81 (2022) 78–91. <https://doi.org/10.1016/j.jmapro.2022.06.036>
- [5] L. Lizzul, R. Bertolini, A. Ghiotti, and S. Bruschi, Turning of Additively Manufactured Ti6Al4V: Effect of the Highly Oriented Microstructure on the Surface Integrity, *Materials* 14 (2021) 2842. <https://doi.org/10.3390/ma14112842>
- [6] L. Lizzul, M. Sorgato, R. Bertolini, A. Ghiotti, and S. Bruschi, Influence of additive manufacturing-induced anisotropy on tool wear in end milling of Ti6Al4V, *Tribology International* 146 (2020) 106200. <https://doi.org/10.1016/j.triboint.2020.106200>
- [7] P. Guo, B. Zou, C. Huang, and H. Gao, Study on microstructure, mechanical properties and machinability of efficiently additive manufactured AISI 316L stainless steel by high-power direct laser deposition, *Journal of Material Research and Technology* 240 (2017) 12–22. <https://doi.org/10.1016/j.jmatprotec.2016.09.005>
- [8] M. Wang, B. Song, Q. Wei, Y. Zhang, Y. Shi, Effects of annealing on the microstructure and mechanical properties of selective laser melted AlSi7Mg alloy, *Materials Science and Engineering A* 739 (2019) 463–472. <https://doi.org/10.1016/j.msea.2018.10.047>
- [9] BS EN ISO 25178-2:2022: Geometrical product specifications (GPS). Surface texture: Areal. Terms, definitions and surface texture parameters.
- [10] Z. Dong, Y. Liu, W. Wen, J. Ge, J. Liang, Effect of Hatch Spacing on Melt Pool and As-built Quality During Selective Laser Melting of Stainless Steel: Modeling and Experimental Approaches, *Materials* 12 (2019) 50. <https://doi.org/10.3390/ma12010050>
- [11] M. Xia, D. Gu, G. Yu, D. Dai, H. Chen, Q. Shi, Influence of hatch spacing on heat and mass transfer, thermodynamics and laser processability during additive manufacturing of Inconel 718 alloy, *International Journal of Machine Tools and Manufacture* 109 (2016) 147–157. <https://doi.org/10.1016/j.ijmachtools.2016.07.010>
- [12] L. Tonelli, E. Liverani, A. Morri, L. Ceschini, Role of Direct Aging and Solution Treatment on Hardness, Microstructure and Residual Stress of the A357 (AlSi7Mg0.6) Alloy Produced by Powder Bed Fusion, *Metallurgical and Materials Transactions B* 52 (2021) 2484–2496. <https://doi.org/10.1007/s11663-021-02179-6>
- [13] E. Simonetto, R. Bertolini, A. Ghiotti, S. Bruschi, Mechanical and microstructural behaviour of AA7075 aluminium alloy for sub-zero temperature sheet stamping process, *International Journal of Mechanical Sciences* 187 (2020) 105919. <https://doi.org/10.1016/j.ijmecsci.2020.105919>